Assessing the controllability of Arctic sea ice extent by sulfate aerosol geoengineering

L. S. Jackson[1], J. A. Crook[1], A. Jarvis[2], D. Leedal[2], A. Ridgwell[3], N. Vaughan[4], and P. M. Forster[1]

[1]Institute for Climate and Atmospheric Science, School of Earth and Environment, University of Leeds, Leeds, UK, [2]Lancaster Environment Centre, Lancaster University, Lancaster, UK, [3]School of Geographical Sciences, University of Bristol, Bristol, UK, [4]Tyndall Centre for Climate Change Research, School of Environmental Sciences, University of East Anglia, Norwich, UK

Abstract In an assessment of how Arctic sea ice cover could be remediated in a warming world, we simulated the injection of SO_2 into the Arctic stratosphere making annual adjustments to injection rates. We treated one climate model realization as a surrogate "real world" with imperfect "observations" and no rerunning or reference to control simulations. SO_2 injection rates were proposed using a novel model predictive control regime which incorporated a second simpler climate model to forecast "optimal" decision pathways. Commencing the simulation in 2018, Arctic sea ice cover was remediated by 2043 and maintained until solar geoengineering was terminated. We found quantifying climate side effects problematic because internal climate variability hampered detection of regional climate changes beyond the Arctic. Nevertheless, through decision maker learning and the accumulation of at least 10 years time series data exploited through an annual review cycle, uncertainties in observations and forcings were successfully managed.

1. Introduction

September Arctic sea ice (ASI) area decreased by $12.2 \pm 1.3\%$ per decade during 1979–2013 [*Fetterer et al.*, 2002]. Climate models project that this decline in ASI area will continue during the 21st century, with ice free conditions in September likely to occur between 2032 and 2046 [*Snape and Forster*, 2014]. This has important far-field consequences because ASI area is strongly coupled with surface air temperature (SAT) in the Northern Hemisphere high latitudes [*Kumar et al.*, 2010] and anthropogenic warming is amplified by surface albedo feedback [*Winton*, 2006].

Assuming mitigation policies prove ineffective or slow to take effect, geoengineering Earth's climate by solar radiation management (SRM) could potentially be used to temporarily reduce the impact of anthropogenic climate change [*Budyko*, 1977; *Crutzen*, 2006]. The injection of aerosols or precursor gases into the stratosphere could potentially cool the global climate through attenuation of incoming solar radiation [e.g., *Niemeier et al.*, 2013] reducing shortwave energy input to the climate system. However, geoengineering need not be carried out solely to achieve global scale climate cooling, and specific regional climate remediation targets [e.g., *Irvine et al.*, 2009] may be achievable by the active management of regional-scale injections [*Robock et al.*, 2008; *MacCracken et al.*, 2013]. Indeed, the same positive climate feedback that exacerbates ASI decline should enhance any cooling effect caused by SRM and potentially make SRM an effective strategy for temporary remediation of the ASI [e.g., *Robock et al.*, 2008].

Previous climate model studies have shown that the ASI area could be restored by SRM [*Jones et al.*, 2010; *Tilmes et al.*, 2014]. While these studies have focused on the possible climate impacts, they have not addressed how the management of SRM deployment might work in practice. For example, they typically assume fixed rates of geoengineering injection for a fixed period of time [e.g., *Kravitz et al.*, 2011]. Further, impacts are usually analyzed by comparison to a no-geoengineering control simulation, something not available in real world deployment, leading to a difference in knowledge available from paired model experiments and a real world situation.

In this study, we explore the practical challenges posed by SRM deployment through a simulation exercise. We treat one realization of the Hadley Centre Global Environmental Model, version 2 (HadGEM2) climate model as a surrogate "real world" in which the loss of ASI is to be remediated by SRM. To enhance realism, the "real world" simulation included stochastic volcanic eruptions and, to mimic the imperfect observation of climate state, data uncertainties were applied to HadGEM2 outputs. We assume technologies exist at a

sufficient scale to inject SO_2 into the lower stratosphere, within the capability of current tanker aircraft [*Robock et al.*, 2009; *McClellan et al.*, 2012], and from a single point source in the Arctic. No reference was made to a no-geoengineering control simulation or to other HadGEM2 integrations. Like *Kravitz et al.* [2014], we approached this simulation "blind," i.e., without the benefit of having performed it previously. Further, we used a second climate model and model predictive control (MPC) to specify optimal SRM trajectories. Our second climate model was intentionally much simpler than our surrogate "real world" mimicking the imperfect modeling of Earth's climate by the latest generation of climate models.

Any SRM deployment will involve manifold uncertainties. Hence, we exploited MPC [e.g., *Camacho and Bordons*, 2004] to support decision making and the process of learning by doing [*Jarvis and Leedal*, 2012; *MacMartin et al.*, 2014a, 2014b]. MPC is applicable here because decisions are guided by model-based predictions, a key element of the current climate change science paradigm. Furthermore, the review cycle used in MPC to reevaluate model predictions, after only the first steps of a forecast policy are implemented, emulates the process of analysis and update of climate model projections in the light of new observations and learning [e.g., *Leedal et al.*, 2014]. Importantly, persistent climate model errors like the failure to simulate the Northern Hemisphere dynamical response to volcanic eruptions [*Driscoll et al.*, 2012] would be captured by an MPC learning process.

2. Models

2.1. HadGEM2-CCS as a Surrogate "Real World"

For our "real world" simulation, we used a fully coupled atmosphere-ocean general circulation model, HadGEM2-CCS [*Collins et al.*, 2008; *Martin et al.*, 2011], that includes processes for sea ice, ocean geochemistry, and the terrestrial carbon cycle. The model atmosphere has 60 vertical levels extending to 84.5 km altitude which provides enhanced representation of stratospheric dynamics and radiation and a horizontal resolution of 1.25° latitude by 1.875° longitude. The model ocean has 40 vertical levels, a 1° longitude resolution and a latitude resolution of 1° between the poles and 30°N/S which increases to 1/3° at the equator. The sulfate aerosol scheme divides sulfate aerosol into three modes: Aitken, accumulation, and dissolved modes [*Jones et al.*, 2001; *Bellouin et al.*, 2007]. The scheme includes gaseous phase oxidation of SO_2 to H_2SO_4 in the stratosphere via reactions with the hydroxyl radical. It incorporates stratosphere/troposphere aerosol gravitational sedimentation, the growth of aerosols and transitions between modes, loss of sulfate aerosol through precipitation, and the interaction of sulfate aerosol with atmospheric radiation and cloud microphysics. In a previous simulation of the 1979–2011 trends in ASI, HadGEM2 compared well with observations, i.e., within 1 standard deviation [*Stroeve et al.*, 2012].

2.2. Model Predictive Control and Sequential Decision Making

An MPC algorithm was used to determine the annual SO_2 injections required to achieve the ASI target. The MPC algorithm was run outside of HadGEM2. Its predictive component was a simplified version of the MAGICC2.0 simple climate model [*Den Elzen and Lucas*, 2003; *Meinshausen et al.*, 2011] extended to simulate the effects of hemispheric SO_2 injections on radiative forcing and the subsequent effect of this on ASI area. Parameters relating SO_2 injections to global radiative forcing and relating changes in annual mean Northern Hemisphere temperature to changes in ASI area were calibrated using results from the Coupled Model Intercomparison Project 5 climate model simulations (excluding HadGEM2) [*Taylor et al.*, 2012] and historic time series of temperature and sea ice from the "real world" simulation (see supporting information).

3. Simulation Design

We ran two simulations, "real world" ("RW") with the MPC algorithm guiding SO_2 injections and a no-geoengineering control ("CTRL") which differed only in the absence of SRM. CTRL was used for analysis after completion of RW and was not used in the management of SRM injections.

The simulations started from 1 January 2018 using an initial climate state spun-up with natural and anthropogenic forcings for the period 1860–2005 and Representative Concentration Pathways 4.5 (RCP4.5) [*Moss et al.*, 2010] for 2006–2017. Future greenhouse gas and aerosol concentrations were based on RCP4.5. Forcing from future explosive volcanic eruptions was included. It is unpredictable, irregular, and potentially large, presenting a

different challenge to the MPC algorithm and decision making than the more gradual changes in greenhouse gas and aerosol concentrations (see supporting information).

SRM in RW involved the simulated injection of SO_2 in the atmosphere above Svalbard (11°56′E, 78°55′N) at an altitude of 14.5 km in a layer approximately 1 km deep. SO_2 injections were timed to maximize attenuation of incoming solar radiation (see supporting information). To simulate the effect of "technological failures," downtime was simulated by randomly missing a monthly injection in March and deferring it to April.

The simulation was paused at the end of each calendar year and a review cycle used to reevaluate the scheduled SO_2 injection rates in the light of observed performance. Annual mean hemispheric temperatures, annual minimum ASI area, estimated greenhouse gas and anthropogenic aerosol forcings, estimated stratospheric SO_2 emissions from volcanic eruptions, and SO_2 geoengineering injections for the previous year were input into the MPC algorithm (see supporting information for data and Figure S1). Greenhouse gas forcing was estimated using an Intergovernmental Panel on Climate Change approximation [*Ramaswamy et al.*, 2001], and negative aerosol forcing was estimated assuming a simple linear relation with greenhouse gas forcing (see supporting information). Performance of the MPC SO_2 injections was reviewed by comparing RW annual minimum ASI area against target (see below) and by attempting to identify climate side effects associated with SRM. The simulation was then restarted with revised SO_2 injection rates and run for the next calendar year.

To include the effects of imperfections in observations, noise was added to HadGEM2 outputs for temperature, sea ice, and top of atmosphere (TOA) energy fluxes (see supporting information). During the RW simulation, time series data were available for analysis for hemispheric mean temperatures (from 1860), ASI area (from 1970), and TOA radiation fluxes (from 2010). The detection of side effects, without use of CTRL, was based on the comparison of a decadal mean climatology for the period immediately before SO_2 injections and decadal periods during geoengineering.

The ASI target was set at the mean RW 1970–2005 annual minimum area, to be achieved by 2050. During 2018 to 2050, the annual target increased gradually starting from the 2018 RW ASI area. To test the statistical significance of regional variations in RW and CTRL that persisted until the 2090s, we ran two additional ensemble runs for RW and CTRL starting from a perturbed 1 January 2075 climate state.

4. Results

4.1. The "Real World" Simulation

Annual minimum ASI area in RW had contracted to a historic low by 2015 and declined at $11.6 \pm 3.7\%$ per decade from 1997 to 2017. Immediately after 2018 (Figure 1 (time interval a)) when SRM could have been deployed, the ASI area was close to the initial target of ~3.0 million km^2 and the MPC algorithm suggested that no SRM intervention was necessary. We followed the MPC recommendations even when, from 2023, ASI continued its longer-term downward trend. In our annual reviews, we concluded that more years data were required for us to clearly establish that changes to the MPC algorithm were necessary. The MPC algorithm did not respond with geoengineering injections until 2026 and even after 2026, when the deficit against target widened (Figure 1 (interval b)), the magnitude of the SO_2 injections suggested by the MPC algorithm increased more slowly than expected. We expected Northern Hemisphere temperature must cool for ASI area to expand: Northern Hemisphere temperature was roughly stable from 2027 to 2038 adding to our concerns that SO_2 injections were too small.

At the end of 2038, we intervened in the control of SO_2 injections. We amended the MPC algorithm parameters to reflect emerging results since 2018 and redistributed SO_2 injections over the first 21 weeks of each year, varying them weekly (see supporting information). We also concluded that net anthropogenic forcing was likely underestimated based on a judgment that anthropogenic aerosol forcing was reducing in the 2030s and by analysis of RW TOA radiation fluxes. We, therefore, changed our estimation of anthropogenic aerosol forcing in the MPC algorithm from a simple linear relationship dependent on greenhouse gas forcing to an estimate based on the RW net TOA radiation balance (see supporting information).

We implemented these changes to the MPC algorithm from January 2039 and adopted the increased SO_2 injection rates recommended by the MPC algorithm. During 2039 to 2043 (Figure 1 (interval c)) Northern
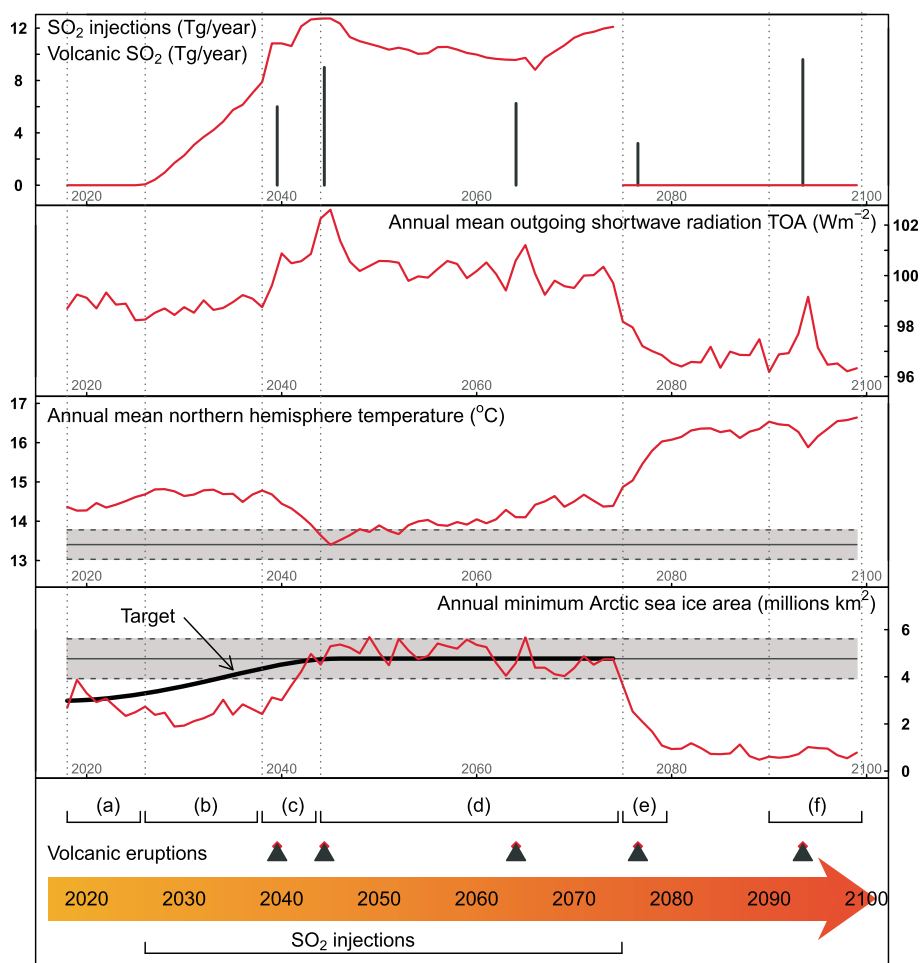
Figure 1. Time series for RW (red lines), volcanic SO_2 emissions (gray bars), 1970–2005 mean with its 95% confidence interval (solid gray line with gray shading), and 2018–2074 geoengineering sea ice target (black line).

Hemisphere temperature cooled, and annual minimum ASI area expanded rapidly to achieve the target level in 2043. However, cause and effect could not be uniquely determined as the MPC change coincided with the occurrence of a volcanic eruption in 2039 and a random technological failure in 2039 (which also occurred in 2028 and 2055).

We sustained SO_2 injections during 2044–2074 (Figure 1 (interval d)). Injections peaked in 2045 at 12.7 Tg [SO_2] requiring a maximum rate of injection of 0.9 Tg[SO_2]/week. Following a second volcanic eruption in 2044, a further change was made to the MPC algorithm to improve its estimation of radiative forcing for SO_2 injections (see supporting information).

In 2074, we stopped geoengineering. The ASI area contracted immediately (Figure 1 (interval e)), and we speculated that the geoengineered expansion of ASI area was reversed by 2080. During the 5 years after termination of SO_2 injections, the rate of increase in Northern Hemisphere annual mean SAT accelerated to $0.33 \pm 0.02°C/yr$. By the 2090s (Figure 1 (interval f)) the annual minimum ASI area had stabilized at 0.74 ± 0.18 million km^2, and Northern Hemisphere annual mean SAT ceased to show any clear trend.

To identify the impact of SO_2 injections on SAT beyond the Arctic region, without reference to CTRL, we compared decadal mean SAT during injections against decadal mean SAT for the decade immediately prior to injections. As an illustration, Figure 2a shows the difference in temperature between 2065–2074 and 2016–2025. We interpreted warming in the Southern Hemisphere as predominantly anthropogenic climate change, cooling in the Northern Hemisphere as a side effect of SRM, and Northern Hemisphere regions without significant changes were interpreted as SRM offsetting the RCP4.5 forcing.
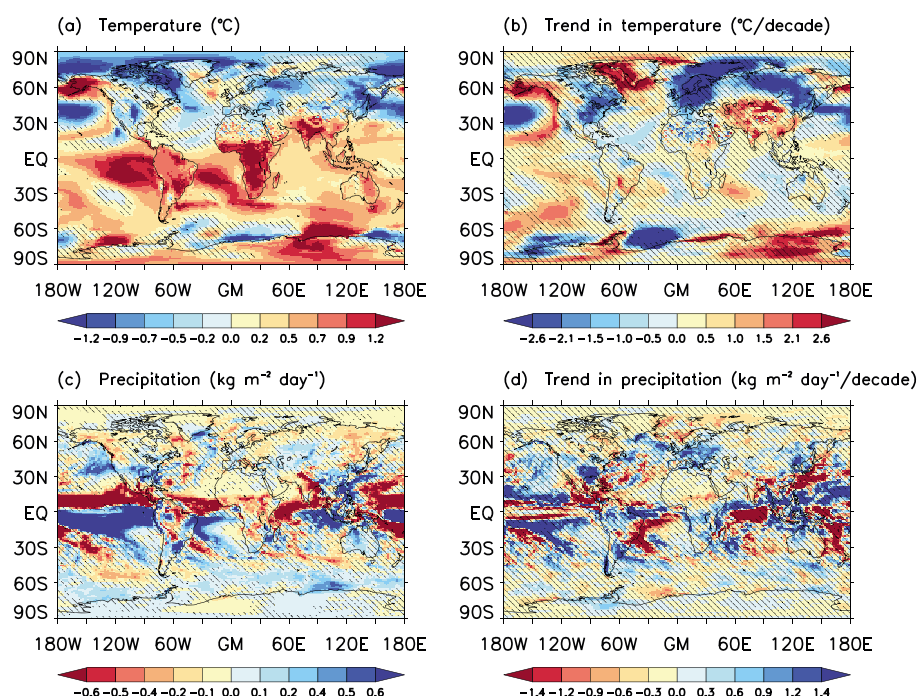
Figure 2. Differences in RW between 2065–2074 and 2016–2025 for (a) decadal mean surface air temperature, (b) trend in surface air temperature, (c) decadal mean precipitation, and (d) trend in precipitation. Hatching shows differences that are less than 2 standard deviations in the 10 year mean.

To isolate the impact of SO_2 injections on temperature from the impact of RCP4.5 forcing, we calculated the difference between annual mean SAT during 2065–2074 and 2016–2025 and used linear regression to determine a trend (Figure 2b). Assuming the SAT trend associated with RCP4.5 forcing was identical in both periods, then any trend in the differences will show the temperature trend attributable to SO_2 injections. It was difficult to identify statistically significant trends for many regions, although eastern North American, most of Europe, and large swathes of Russia showed strong cooling trends in the midlatitudes that we associated with SRM. Warming trends in the Northern Hemisphere (e.g., India, China, and central Asia) were interpreted as likely a combination of relatively weak cooling from Arctic SO_2 injections, and enhanced warming under RCP4.5 possibly linked to reduced anthropogenic aerosol emissions.

Figure 2c shows the difference in annual mean precipitation between 2065–2074 and 2016–2025. Southward migration of the intertropical convergence zone and annual mean tropical precipitation over the Atlantic and Indian Oceans accompanied drying of equatorial Africa, including the Sahel, and central/northern regions of India. Wetting south of the equator occurred in the Northeast region of Brazil and Western Australia. The linear trend in the difference between annual mean precipitation in 2065–2074 and 2016–2025 (Figure 2d) did not help us identify regional precipitation side effects associated with SRM. The changes in precipitation varied greatly over small spatial scales and did not satisfy tests of statistical significance.

4.2. Comparison of Surrogate "Real World" and Control Simulations

On completion of RW, we compared RW against CTRL retrospectively to quantify more accurately the impacts and side effects of SRM and assess our decision making. During SO_2 injections (Figure 3 (time interval a)), SRM was the dominant factor driving the temporary recovery of annual minimum ASI and the reduction in Northern Hemisphere annual mean SAT to year 2045. SRM also impacted SAT beyond the Arctic region as shown by the reduced rate of increase in annual mean Southern Hemisphere SAT during 2038–2074 when SO_2 injections were large. The annual maximum ASI area, which occurred in March, also responded to SO_2 injections but resumed its declining trend after its peak in 2052.

During the 5 years, immediately after stopping SRM, there was a temporary acceleration in the rate of decline of annual maximum and minimum ASI area and accelerated warming of both hemispheres not seen in CTRL (Figure 3 (interval b)). ASI area was greater in RW than CTRL in the 2090s. The difference in annual maximum
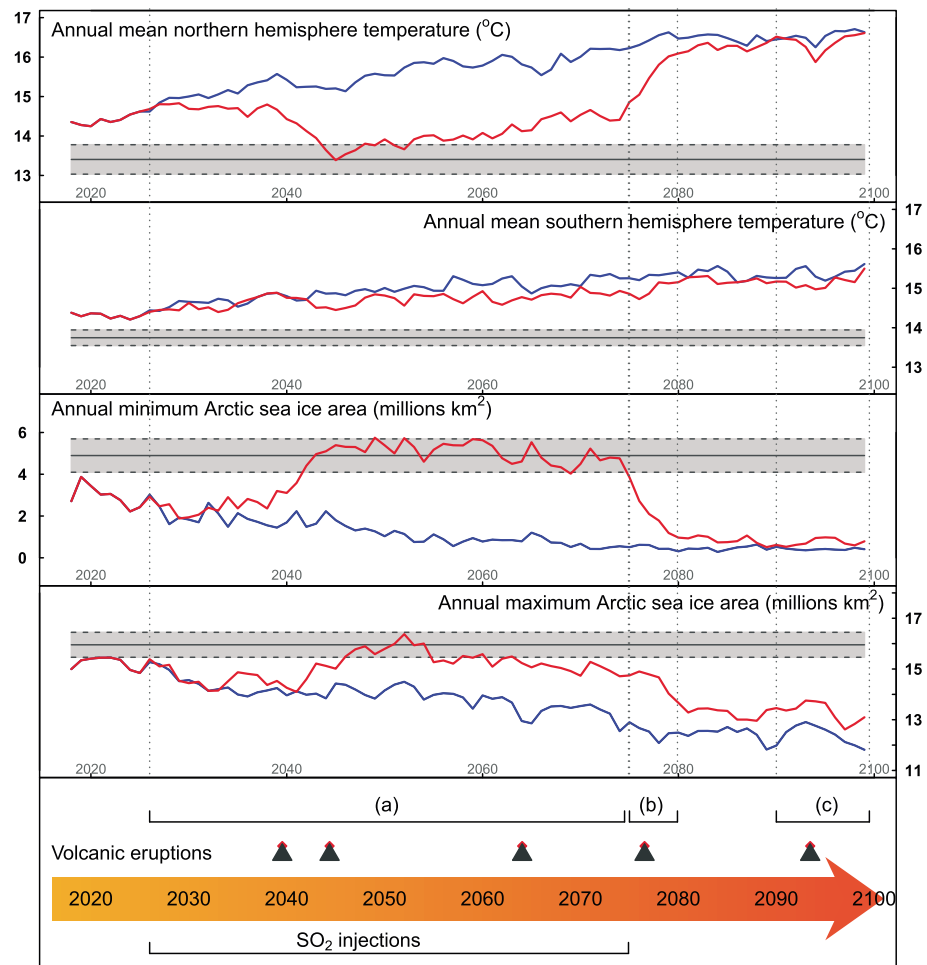
Figure 3. Time series RW (red lines), CTRL (blue lines), and 1970–2005 mean with its 95% confidence interval (solid gray line with gray shading).

sea ice area was statistically significant at the 5% level using a *t* test and likely associated with the Northern Hemisphere annual mean SAT which remained cooler in RW than CTRL (Figure 3 (interval c)).

The difference between 2065–2074 decadal mean SAT for RW and CTRL (Figure 4a) confirms that SO_2 injections cooled almost all the Northern Hemisphere and Southern Hemisphere land as well as the Arctic. To assess side effects of Arctic SRM, we assigned grid cell outcomes for RW land to one of four categories (Figure 4b):

1. "Insignificant" where RW climate was within 2 standard deviations of CTRL climate;
2. "Effective" where RW climate was within 2 standard deviations of the 2016–2025 decadal mean, the decade immediately prior to commencement of SO_2 injections, otherwise;
3. "Marginally effective" where RW climate was between CTRL and the 2016–2025 decadal mean, or finally;
4. "Damaging" where RW climate resided outside the range bounded by the 2016–2025 decadal mean and the CTRL climate and more than 2 standard deviations away from both.

Effective side effects in SAT covered less than half the global land area and were not equitably distributed. Damaging changes, however, almost completely avoided continental regions.

SAT side effects persisted until the 2090s (Figure 4c), and the RW global field of 2090–2099 decadal mean temperature was significantly different from CTRL at the 5% level using the field significance test of *Livesey and Chen* [1983]. Land areas marked by hatching in Figure 4c were either significantly cooler in all three ensemble runs (parts of Canada and Australia) or significantly warmer in all ensemble runs (UK). These areas differ, however, from the regions of damaging temperature change (Figure 4d). A larger ensemble of runs
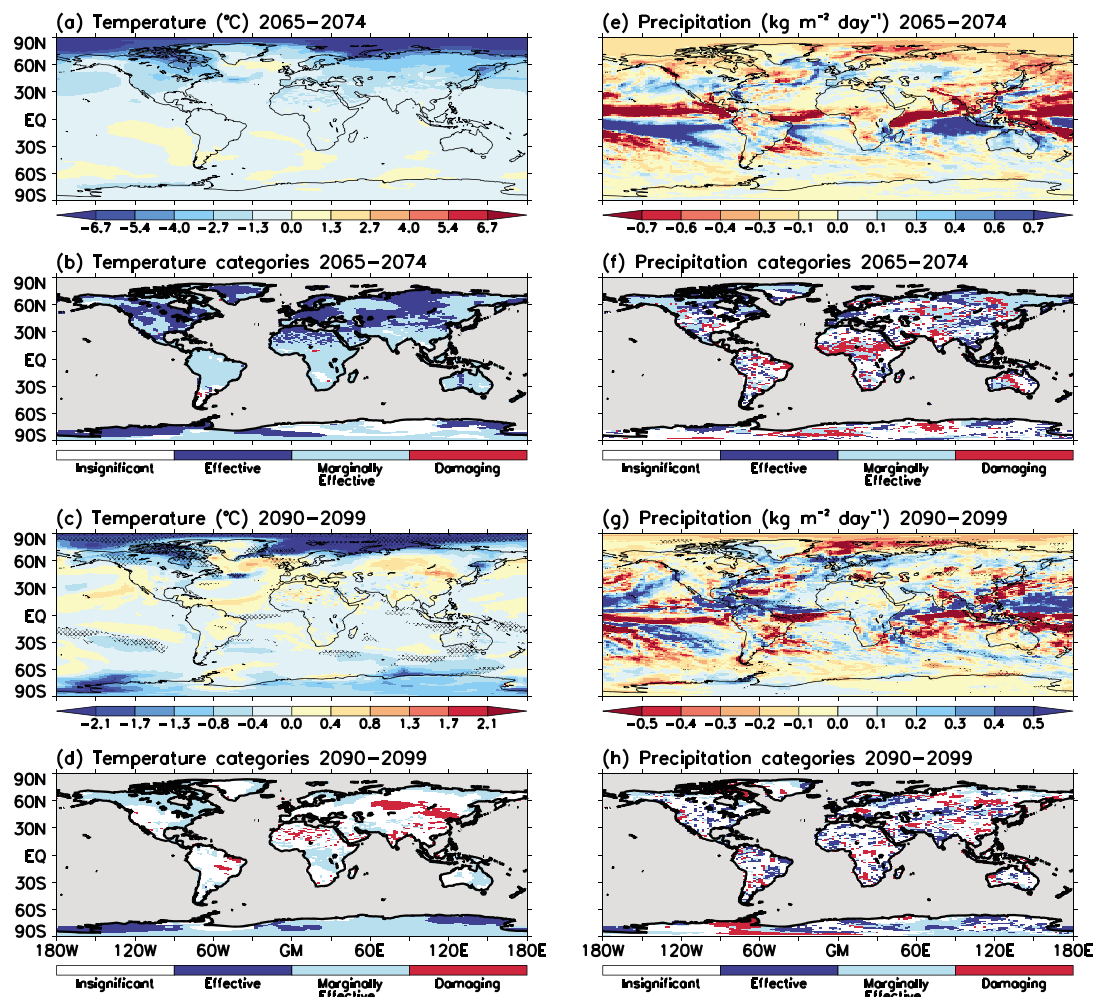
Figure 4. (a, c, e, and g) Difference between decadal means for RW and CTRL simulations. Hatching shows grid cells significant in all three postgeoengineering ensemble runs (Figures 4c and 4g). (b, d, f, and h) Categories assigned to decadal means for RW land when compared with CTRL and the 2016–2025 climatology.

would be required to determine the location and spatial extent of any statistically significant damaging temperature changes.

Cooling of the Arctic during 2065–2074 was accompanied by a 1.7% reduction in global mean precipitation over land and oceans. A 7.4% decrease in Northern Hemisphere precipitation, coupled with a 1.5°C decrease in Northern Hemisphere SAT, was accompanied by a 3.9% increase in Southern Hemisphere precipitation principally due to the southward migration of maritime tropical precipitation (Figure 4e). Statistically significant changes in 2065–2074 decadal mean precipitation for RW land compared to CTRL were widespread but spatially irregular (Figure 4f). Notable changes over land include damaging drying in the Sahel, northern India, and regionally in the Amazon.

Decadal mean global precipitation in RW recovered by the 2090s to within 2 standard deviations of CTRL although the field of regional differences (Figures 4g and 4h) remained significant at the 5% level using the test of *Livesey and Chen* [1983]. The location of these differences, however, was more uncertain than for SAT with a smaller number of grid cells significant in all three ensemble runs for the 2090s.

5. Discussion and Conclusions

While remediation of ASI has previously been demonstrated by *MacCracken et al.* [2013] and *Tilmes et al.* [2014], our simulation incorporated real world uncertainties in observations and active management of SO$_2$ injections without reference to a no-geoengineering control simulation.

Our annual reviews of SO_2 injections and MPC performance focused on attributing changes in ASI area, Northern Hemisphere SAT, and TOA outgoing SW radiation to individual forcings. However, without access to a control simulation, we were not able to isolate the impact of SO_2 injections from other forcings and required at least 10 years of injections before we could detect a clear signal in the ASI changes. This hampered our ability to correct the poor performance of the MPC algorithm in the early years and hindered characterization of the risk that ASI might unexpectedly diverge from target at any point during SRM. Using multiple iterations of the MPC algorithm and many simple climate models for predictions (in addition to MAGICC2.0) would have improved the realism of our simulation and could possibly have contributed to earlier restoration of the ASI area. Detection and attribution of the influence of geoengineering on climate would remain difficult, however, just as it does for all anthropogenic influences on climate [*Stone et al.*, 2009].

Arctic SRM produced widespread changes in precipitation. Cooling was accompanied by a reduction in global precipitation as previously shown by *Niemeier et al.* [2013]. In common with *MacCracken et al.* [2013] and *Tilmes et al.* [2014], we found Arctic SRM caused a shift of tropical maritime precipitation from the Northern Hemisphere toward the Southern Hemisphere. This mimicked the impact of volcanic cooling of the Northern Hemisphere during the twentieth century [*Haywood et al.*, 2013]. Changes in regional precipitation over land varied greatly. In some regions (e.g., parts of Western Europe), precipitation was restored to its pregeoengineering climate mean (2016–2025). In other regions (e.g., the Sahel and India) drying was so great that precipitation was significantly below the regional pregeoengineering climate mean. The spatial pattern of precipitation changes is highly uncertain as our results, by design, are based on just one climate model realization. Unfortunately, even globally uniform SRM interventions [e.g., *Berdahl et al.*, 2014; *Ammann et al.*, 2010] suffer regional side effects. Further, they typically fail to prevent the decline in ASI area because CO_2 has a greater amplification of Arctic temperature change than SRM [*Berdahl et al.*, 2014; *Lunt et al.*, 2008].

Our injection amounts (up to 12 Tg[SO_2]/yr) were large, equivalent to more than 50% of the SO_2 emissions from the 1991 Mount Pinatubo eruption [*Guo et al.*, 2004], and would require more than 1000 KC-135 tanker aircraft flights per day during peak injection periods [*Robock et al.*, 2009]. It remains uncertain whether the stratospheric aerosol concentration would increase linearly with injection rate [*Heckendorn et al.*, 2009] and whether an efficient distribution of aerosol particle size could be sustained [*Niemeier et al.*, 2011]. Accelerated climate change on termination of SRM, also demonstrated by *Jones et al.* [2013], shows climate to be vulnerable to unplanned disruption of SRM injections [*Baum et al.*, 2013]. We found statistically significant differences in regional climate persisted into the 2090s even when global mean climate had returned close to the nongeoengineered state.

In conclusion, we found that ASI was successfully controlled in our simulation, and uncertainties in observations and forcings were effectively managed once decision makers had acquired sufficient experience and once a minimum of 10 years time series data were available. Nevertheless, attribution of climate side effects in real time was very uncertain, even speculative.

References

Ammann, C. M., W. M. Washington, G. A. Meehl, L. Buja, and H. Teng (2010), Climate engineering through artificial enhancement of natural forcings: Magnitudes and implied consequences, *J. Geophys. Res.*, *115*, D22109, doi:10.1029/2009JD012878.

Baum, S. D., T. M. Maher Jr., and J. Haqq-Misra (2013), Double catastrophe: Intermittent stratospheric geoengineering induced by societal collapse, *Environ. Syst. Decis.*, *33*(1), 168–180.

Bellouin, N., O. Boucher, J. Haywood, C. Johnson, A. Jones, J. Rae, and S. Woodward (2007), Improved representation of aerosols for HadGEM2, *Hadley Centre Tech. Note 73*, Met Office Hadley Centre for Climate Change, Exeter, U. K.

Berdahl, M., A. Robock, D. Ji, J. C. Moore, A. Jones, B. Kravitz, and S. Watanabe (2014), Arctic cryosphere response in the Geoengineering Model Intercomparison Project G3 and G4 scenarios, *J. Geophys. Res. Atmos.*, *119*, 1308–1321, doi:10.1002/2013JD020627.

Budyko, M. I. (1977), *Climatic Changes*, 261 pp., AGU, Washington, D. C.

Camacho, E. F., and C. Bordons (2004), *Model Predictive Control*, 2nd ed., 405 pp., Springer, London.

Collins, W. J., et al. (2008), Evaluation of the HadGEM2 model, *Hadley Centre Tech. Note 74*, Met Office, Exeter, U. K.

Crutzen, P. (2006), Albedo enhancement by stratospheric sulphur injections: A contribution to resolve a policy dilemma?, *Clim. Change*, *77*, 211–219, doi:10.1007/s10584-006-9101-y.

Den Elzen, M. G. J., and P. Lucas (2003), FAIR 2.0-A decision-support tool to assess the environmental and economic consequences of future climate regimes, *RIVM-report 550015001*. [Available at www.mnp.nl/fair.]

Driscoll, S., A. Bozzo, L. J. Gray, A. Robock, and G. Stenchikov (2012), Coupled Model Intercomparison Project 5 (CMIP5) simulations of climate following volcanic eruptions, *J. Geophys. Res.*, *117*, D17105, doi:10.1029/2012JD017607.

Fetterer, F., K. Knowles, W. Meier, and M. Savoie (2002), Sea ice index G02135/north/daily, Natl. Snow and Ice Data Cent., Boulder, Colo., doi:10.7265/N5QJ7F7W. [Updated daily.]

Guo, S., G. J. S. Bluth, W. I. Rose, I. M. Watson, and A. J. Prata (2004), Re-evaluation of SO_2 release of the 15 June 1991 Pinatubo eruption using ultraviolet and infrared satellite sensors, *Geochem. Geophys. Geosyst.*, *5*, Q04001, doi:10.1029/2003GC000654.

Haywood, J. M., A. Jones, N. Bellouin, and D. Stephenson (2013), Asymmetric forcing from stratospheric aerosols impacts Sahelian rainfall, *Nat. Clim. Change*, doi:10.1038/nclimate1857.

Heckendorn, P., D. Weisenstein, S. Fueglistaler, B. P. Luo, E. Rozanov, M. Schraner, L. W. Thomason, and T. Peter (2009), The impact of geoengineering aerosols on stratospheric temperature and ozone, *Environ. Res. Lett.*, *4*, 045108, doi:10.1088/1748-9326/4/4/045108.

Irvine, P. J., D. J. Lunt, E. J. Stone, and A. Ridgwell (2009), Fate of the Greenland Ice Sheet in a geoengineered, high CO_2 world, *Environ. Res. Lett.*, *4*, 045109, doi:10.1088/1748-9326/4/4/045109.

Jarvis, A., and D. Leedal (2012), The Geoengineering Model Intercomparison Project (GeoMIP): A control perspective, *Atmos. Sci. Lett.*, *13*, 157–163, doi:10.1002/asl.387.

Jones, A., D. L. Roberts, M. J. Woodage, and C. E. Johnson (2001), Indirect sulfate aerosol forcing in a climate model with an interactive sulphur cycle, *J. Geophys. Res.*, *106*(D17), 20,293–20,310, doi:10.1029/2000JD000089.

Jones, A., J. Haywood, O. Boucher, B. Kravitz, and A. Robock (2010), Geoengineering by stratospheric SO_2 injection: Results from the Met Office HadGEM2 climate model and comparison with the Goddard Institute for Space Studies ModelE, *Atmos. Chem. Phys.*, *10*, 5999–6006, doi:10.5194/acp-10-5999-2010.

Jones, A., et al. (2013), The impact of abrupt suspension of solar radiation management (termination effect) in experiment G2 of the Geoengineering Model Intercomparison Project (GeoMIP), *J. Geophys. Res. Atmos.*, *118*, 9743–9752, doi:10.1002/jgrd.50762.

Kravitz, B., A. Robock, O. Boucher, H. Schmidt, K. E. Taylor, G. Stenchikov, and M. Schulz (2011), The Geoengineering Model Intercomparison Project (GeoMIP), *Atmos. Sci. Lett.*, *12*, 162–167, doi:10.1002/asl.316.

Kravitz, B., D. G. MacMartin, D. T. Leedal, P. J. Rasch, and A. J. Jarvis (2014), Explicit feedback and the management of uncertainty in meeting climate objectives with solar geoengineering, *Environ. Res. Lett.*, *9*, 044006, doi:10.1088/1748-9326/9/4/044006.

Kumar, A., J. Perlwitz, J. Eischeid, X. Quan, T. Xu, T. Zhang, M. Hoerling, B. Jha, and W. Wang (2010), Contribution of sea ice loss to Arctic amplification, *Geophys. Res. Lett.*, *37*, L21701, doi:10.1029/2010GL045022.

Leedal, D., A. Jarvis, and L. S. Jackson (2014), Climate decision-making as a recursive process, paper presented at the joint second International Conference on Vulnerability and Risk Analysis and Management (ICVRAM) and the sixth International Symposium on Uncertainty Modeling and Analysis (ISUMA), ASCE, Liverpool, U. K.

Livesey, R. E., and W. Y. Chen (1983), Statistical field significance and its determination by Monte Carlo techniques, *Mon. Weather Rev.*, *111*, 46–59.

Lunt, D. J., A. Ridgwell, P. J. Valdes, and A. Seale (2008), "Sunshade World": A fully coupled GCM evaluation of the climatic impacts of geoengineering, *Geophys. Res. Lett.*, *35*, L12710, doi:10.1029/2008GL033674.

MacCracken, M. C., H.-J. Shin, K. Caldeira, and G. A. Ban-Weiss (2013), Climate response to imposed solar radiation reductions in high latitudes, *Earth Syst. Dyn.*, *4*, 301–315, doi:10.5194/esd-4-301-2013.

MacMartin, D. G., B. Kravitz, D. W. Keith, and A. Jarvis (2014a), Dynamics of the coupled human–climate system resulting from closed-loop control of solar geoengineering, *Clim. Dyn.*, *43*, 243–258, doi:10.1007/s00382-013-1822-9.

MacMartin, D. G., K. Caldeira, and D. W. Keith (2014b), Solar geoengineering to limit the rate of temperature change, *Philos. Trans. R. Soc. London, Ser. A*, *372*, 20140134, doi:10.1098/rsta.2014.0134.

Martin, G. M., et al. (2011), The HadGEM2 family of Met Office Unified Model climate configurations, *Geosci. Model Dev.*, *4*, 723–757, doi:10.5194/gmd-4-723-2011.

McClellan, J., D. W. Keith, and J. Apt (2012), Cost analysis of stratospheric albedo modification delivery systems, *Environ. Res. Lett.*, *7*, 034019, doi:10.1088/1748-9326/7/3/034019.

Meinshausen, M., S. C. B. Raper, and T. M. L. Wigley (2011), Emulating coupled atmosphere-ocean and carbon cycle models with a simpler model, MAGICC6—Part 1: Model description and calibration, *Atmos. Chem. Phys.*, *11*, 1417–1456, doi:10.5194/acp-11-1417-2011.

Moss, R. H., et al. (2010), The next generation of scenarios for climate change research and assessment, *Nature*, *463*, 747–756, doi:10.1038/nature08823.

Niemeier, U., H. Schmidt, and C. Timmreck (2011), The dependency of geoengineered sulfate aerosol on the emission strategy, *Atmos. Sci. Lett.*, *12*, 189–194.

Niemeier, U., H. Schmidt, K. Alterskjær, and J. E. Kristjánsson (2013), Solar irradiance reduction via climate engineering: Impact of different techniques on the energy balance and the hydrological cycle, *J. Geophys. Res. Atmos.*, *118*, 11,905–11,917, doi:10.1002/2013JD020445.

Ramaswamy, V., O. Boucher, J. Haigh, D. Hauglustaine, J. Haywood, G. Myhre, T. Nakajima, G. Y. Shi, and S. Solomon (2001), Observed climate variability and change, in *Climate Change 2001: The Scientific Basis. Contribution of Working Group I to the Third Assessment Report of the Intergovernmental Panel on Climate Change*, edited by J. T. Houghton et al., pp. 358–359, Cambridge Univ. Press, Cambridge, U. K., and New York.

Robock, A., L. Oman, and G. L. Stenchikov (2008), Regional climate responses to geoengineering with tropical and Arctic SO_2 injections, *J. Geophys. Res.*, *113*, D16101, doi:10.1029/2008JD010050.

Robock, A., A. Marquardt, B. Kravitz, and G. Stenchikov (2009), Benefits, risks, and costs of stratospheric geoengineering, *Geophys. Res. Lett.*, *36*, L19703, doi:10.1029/2009GL039209.

Snape, T. J., and P. M. Forster (2014), Decline of Arctic sea ice: Evaluation and weighting of CMIP5 projections, *J. Geophys. Res. Atmos.*, *119*, 546–554, doi:10.1002/2013JD020593.

Stone, D. A., M. R. Allen, P. A. Stott, P. Pall, S. K. Min, T. Nozawa, and S. Yukimoto (2009), The detection and attribution of human influence on climate, *Annu. Rev. Environ. Resour.*, *34*, 1–16.

Stroeve, J. C., V. Kattsov, A. Barrett, M. Serreze, T. Pavlova, M. Holland, and W. N. Meier (2012), Trends in Arctic sea ice extent from CMIP5, CMIP3 and observations, *Geophys. Res. Lett.*, *39*, L16502, doi:10.1029/2012GL052676.

Taylor, K. E., R. J. Stouffer, and G. A. Meehl (2012), An overview of CMIP5 and the experiment design, *Bull. Am. Meteorol. Soc.*, *93*, 485–498, doi:10.1175/BAMS-D-11-00094.1.

Tilmes, S., A. Jahn, J. E. Kay, M. Holland, and J.-F. Lamarque (2014), Can regional climate engineering save the summer Arctic sea ice?, *Geophys. Res. Lett.*, *41*, 880–885, doi:10.1002/2013GL058731.

Winton, M. (2006), Amplified Arctic climate change: What does surface albedo feedback have to do with it?, *Geophys. Res. Lett.*, *33*, L03701, doi:10.1029/2005GL025244.